ADVANCED ENERGY MATERIALS

Supporting Information

for *Adv. Energy Mater.*, DOI: 10.1002/aenm.201301624

Sponge-Like Piezoelectric Polymer Films for Scalable and Integratable Nanogenerators and Self-Powered Electronic Systems

*Yanchao Mao, Ping Zhao, Geoffrey McConohy, Hao Yang, Yexiang Tong, and Xudong Wang**

Supporting Information

Sponge-like Piezoelectric Polymer Film for Scalable and Integratable Nanogenerators and Self-Powered Electronic Systems

*Yanchao Mao, Ping Zhao, Geoffrey McConohy, Hao Yang, Yexiang Tong, Xudong Wang**

Y. C. Mao, Prof. X. D. Wang
Department of Materials Science and Engineering, University of Wisconsin-Madison, Madison, WI 53706, USA
E-mail: xudong@engr.wisc.edu

Y. C. Mao, H. Yang, Prof. Y. X. Tong
MOE Laboratory of Bioinorganic and Synthetic Chemistry, KLGHEI of Environment and Energy Chemistry, School of Chemistry and Chemical Engineering, Sun Yat-sen University, Guangzhou 510275, China

Prof. P. Zhao
Department of Mechanical Engineering, University of Minnesota-Duluth, Duluth, MN 55812, USA

G. McConohy
Department of Engineering Physics, University of Wisconsin-Madison, Madison, WI 53706, USA

S1. PVDF thin films before and after acid etching

The SEM image of a PVDF thin film before acid etching was shown in Figure S1. The ZnO NPs were uniformly distributed in the matrix of PVDF. The sizes of the ZnO NPs (35-45 nm in average) correspond to the pore sizes of the nanoporous PVDF thin film. The ZnO NPs are also interconnected, which allows ZnO NPs to be completely removed (inset of Figure S1). Figure S2 shows an EDS spectrum of the PVDF thin film after acid etching. Only C and F elements were detected in the thin film, which proved that the ZnO NPs were completely removed. The crystal phase of the PVDF thin film was analyzed by FTIR spectrum, as shown in Figure S3. The peaks at 509, 840 and 1280 cm^{-1} belong to the β-phase PVDF,[1,2] confirming that the piezoelectric *β*-phase PVDF was successful fabricated.

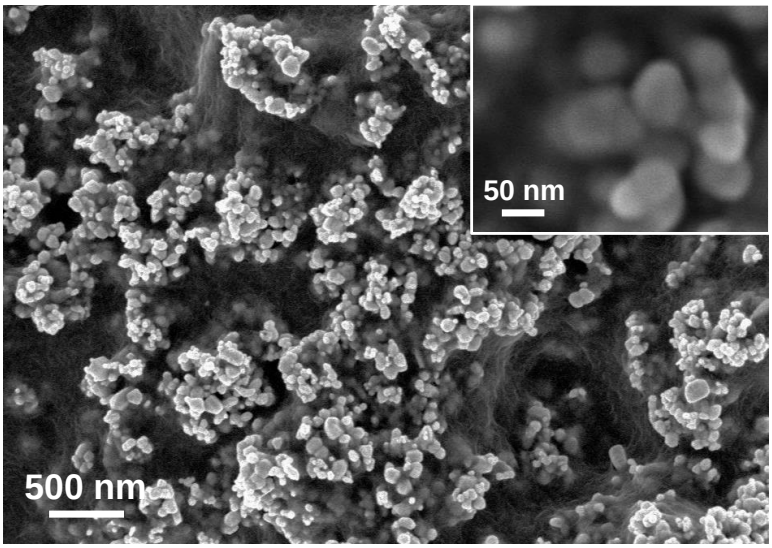

Figure S1. SEM image of the PVDF thin film before etching prepared from a mixture of PVDF and ZnO (50% mass fraction).

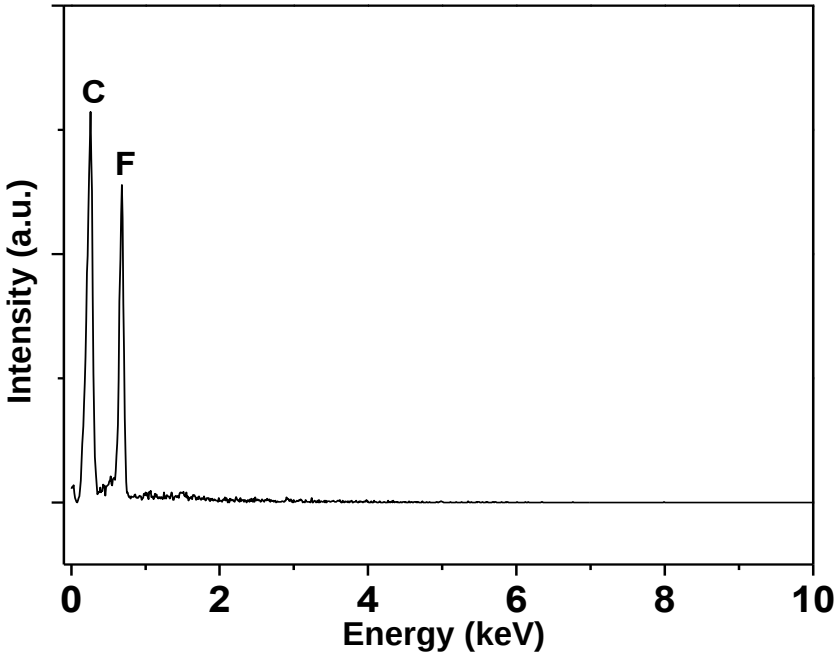

Figure S2. EDS spectrum of the nanoporous PVDF thin film.

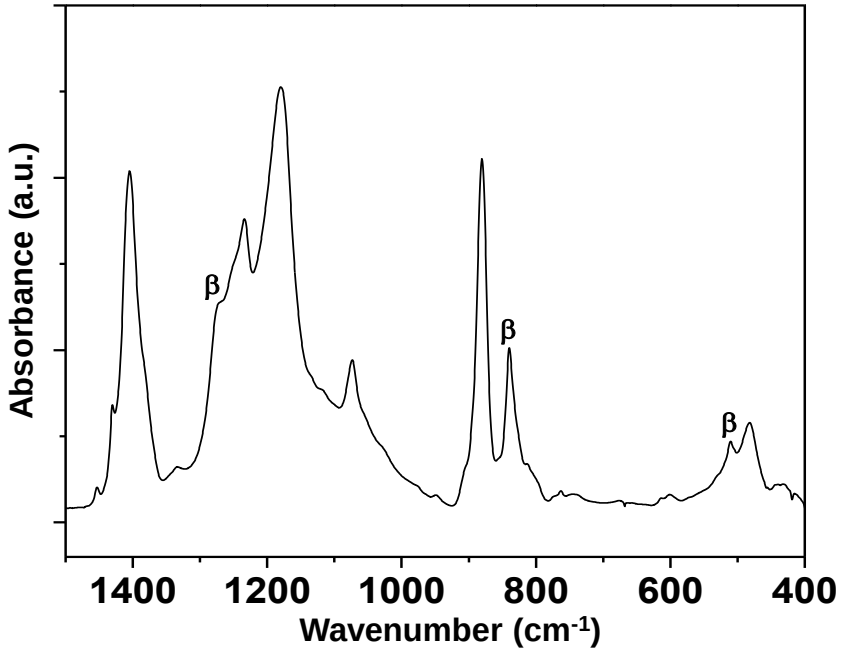

Figure S3. FTIR spectrum of the nanoporous PVDF thin film.

S2. The durability test of the NG

The durability test was conducted to confirm the performance stability of the NG, as shown in Figure S4. The peak V_{OC} output did not appear any noticeable degradation during an operation time of 1 hour under continuous oscillations with a driving frequency of 40 Hz.

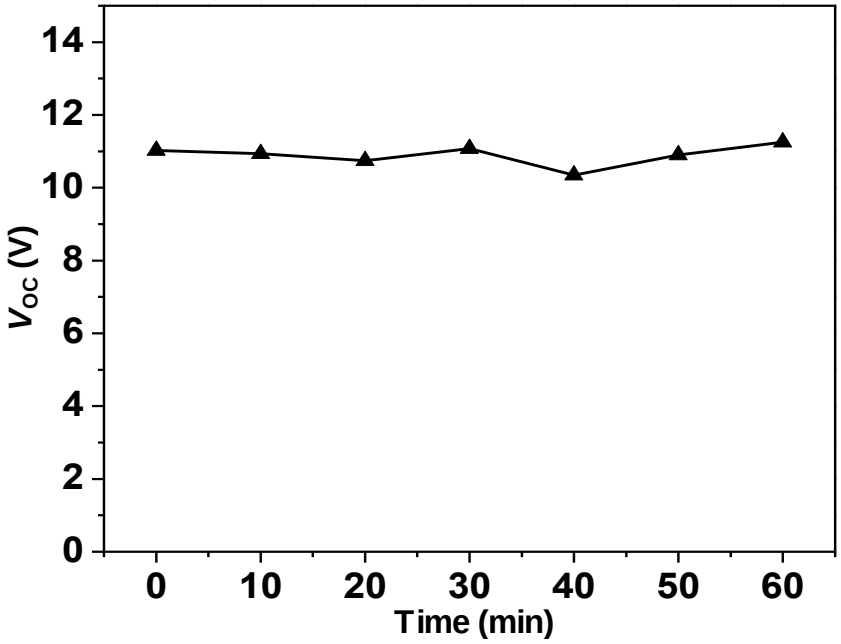

Figure S4. The peak V_{OC} recorded at given time intervals from a PVDF NG under continuous oscillations at a driving frequency of 40 Hz.

S3. PVDF thin films with different porosities

Figures S5a and b show SEM images of the nanoporous PVDF thin films prepared from mixtures with 70% and 10% ZnO mass fraction, respectively. It can be clearly seen that more ZnO NPs in the mixture generated higher porosity in the nanoporous PVDF thin film (Figure S5a). The pores are highly interconnected with each other. As to the PVDF thin film prepared from 10% ZnO mass fraction mixture (Figure S5b), much fewer pores were observed in the matrix of the PVDF thin film after etching.

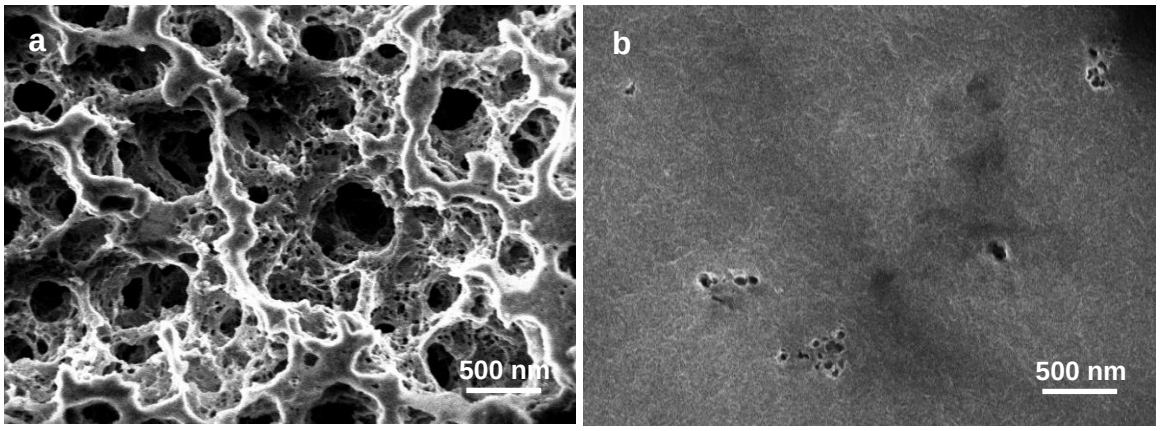

Figure S5. a,b) SEM images of nanoporous PVDF thin films prepared from mixtures with 70% (a) and 10% (b) ZnO mass fraction, respectively.

S4. Phase identification of PVDF thin films with different porosities

The phases of as-fabricated nanoporous PVDF thin films were identified by FTIR spectrum (Figure S6). The peaks at 509, 840 and 1280 cm^{-1} belong to the β-phase, and the peaks at 530, 612, 795 and 975 cm^{-1} are originated from the α-phase.[1,2] The spectra show that the amount of α-phase monotonically decreased as the ZnO ratio increased. At the same time, the amount of β-phase increased as the ZnO mass fraction increased from 10% to 50%, and decreased as the ZnO mass fraction further increased to 70%. The nanoporous PVDF thin film prepared from the 50% ZnO mass fraction mixture demonstrated the strongest characteristic peaks of the β-phase.

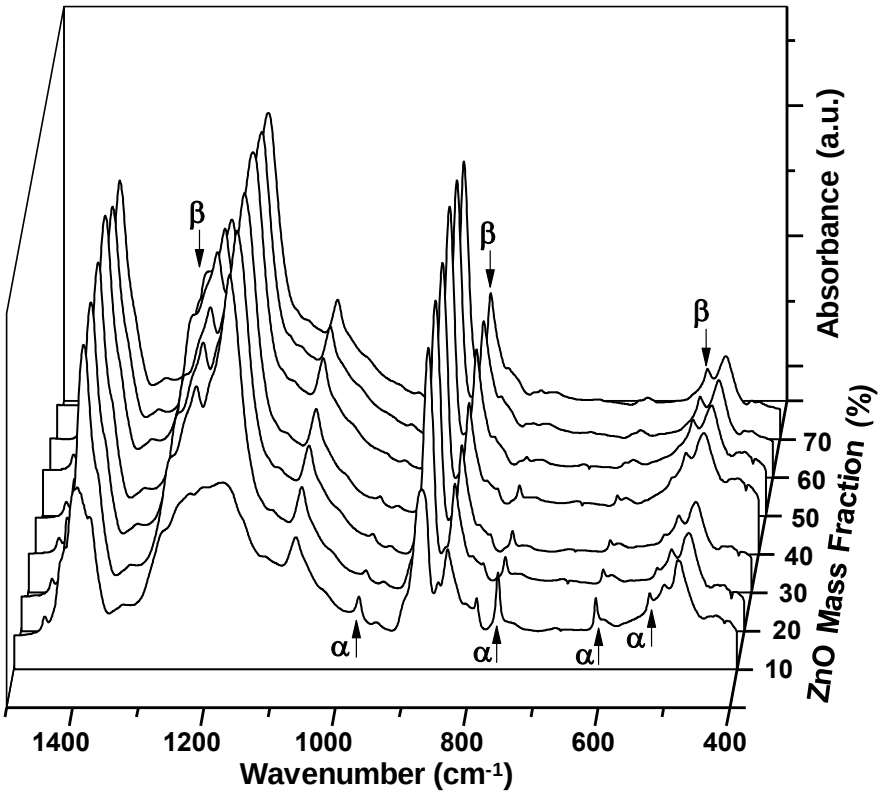

Figure S6. FTIR spectra of PVDF thin films prepared from the mixtures with ZnO mass fraction varied from 10% to 70%.

S5. Calculation of spring constant *K* and and damping ratio *C*

The vibration dynamics is applied to analyze the nanoporous PVDF NGs. In order to find the spring constant *K* and damping ratio *C* of the device, we start with the piezoelectric behavior of PVDF. Piezoelectric materials exhibit a linear behavior under external loading. In the absence of body force and free charge density of a piezoelectric material, the coupled constitutive law indicates the equilibrium both mechanically and electrically. The constitutive equation is given by:

$$\begin{aligned} \sigma_{ij} &= C_{ijkl}^{E}\varepsilon_{kl} - e_{nij}E_n \\ D_m &= e_{mkl}\varepsilon_{kl} + k_{mn}^{\varepsilon}E_n \end{aligned} \qquad (1)$$

where σ_{ij} and ε_{kl} are the stress and strain, E_n and D_m are the electric field and electric displacement, C_{jikl}^{E}, e_{nij} and k_{mn}^{ε} are the elastic (under a constant electric field), piezoelectric, and dielectric tensor (under a constant stress).

In the NG device, strain ε_{kl} induces electric displacement D_m. Thus, the 2nd equation in eq. (1) is used for the calculation. Since no electric field is applied to the device, it can be simplified as

$$D_m = e_{mkl}\varepsilon_{kl} \qquad (2)$$

Thus, the electric displacement along the device thickness direction (the 3 axis) is

$$D_3 = e_{3kl}\varepsilon_{kl} \qquad (3)$$

The strain along the 3 axis ε_{33} makes significant contributions to the electric displacement D_3, so the strains along other directions can be ignored. Eq.(3) turns into

$$D_3 = e_{333}\varepsilon_{33} \qquad (4)$$

where $D_3 = \frac{Q}{A} = \frac{C_p V}{A}$ (Q is charge, C_p is the capacitance of the device, V is the measured voltage from the device, A is the area of the electrode). $\varepsilon_{33} = \frac{x}{d}$ (d is the thickness of the device, x is the displacement of the device).

Substituting D_3 and ε_{33} into eq. (4), it can be rewritten as

$$x = \frac{C_p d}{A e_{333}} V \qquad (5)$$

The operation of nanoporous PVDF NGs with attached electronic device (acts as the proof mass) can be simulated using a vibration dynamics system shown in Figure S7.

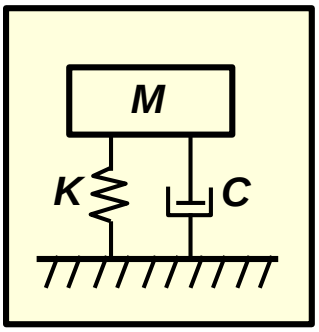

Figure S7. The schematic of the free vibration dynamics system with damping.

The free vibration with damping is given by

$$M\ddot{x} + C\dot{x} + Kx = 0 \qquad (6)$$

where M is the proof mass, x is the displacement, C and K are the damping ratio and spring constant, respectively. Substituting Eq. (5) into Eq. (6) yields:

$$M\frac{C_p d}{Ae_{333}}\ddot{V} + C\frac{C_p d}{Ae_{333}}\dot{V} + K\frac{C_p d}{Ae_{333}}V = 0 \qquad (7)$$

In Eq. (7), the damping ratio C and spring constant K are material's property, and are independent to the constants C_p, d, A and e_{nij} as well as time. Thus, Eq. (7) turns into:

$$M\ddot{V} + C\dot{V} + KV = 0 \qquad (8)$$

Equation (8) is based on the free vibration system with damping and can be applied to analyze the behavior of the nanoporous PVDF NGs. The experimental voltage versus time data of PVDF thin films were input to Eq.(8). The Mathcad 15 software was used to solve the Eq. (8) with a 2nd order ordinary differential equation. Thus, the damping ratio C and spring constant K were obtained. Figure S8 shows the voltage output profiles generated during one cycle of oscillation from nanoporous PVDF thin films fabricated using mixtures with ZnO mass fraction varying from 10% to 70%. The calculated K and C values of the PVDF thin films with different porosities were shown in Table S1. (Note: here the damping ratio describes the total damping including both mechanical and electrical damping. Therefore, it can be marked as C_{total}). The calculation shows that spring constant K decreases and damping ratio C increases as the ZnO mass fraction increases. The results are consistent with the fact that more ZnO particles introduced more pores in the PVDF thin film, which makes the device softer.

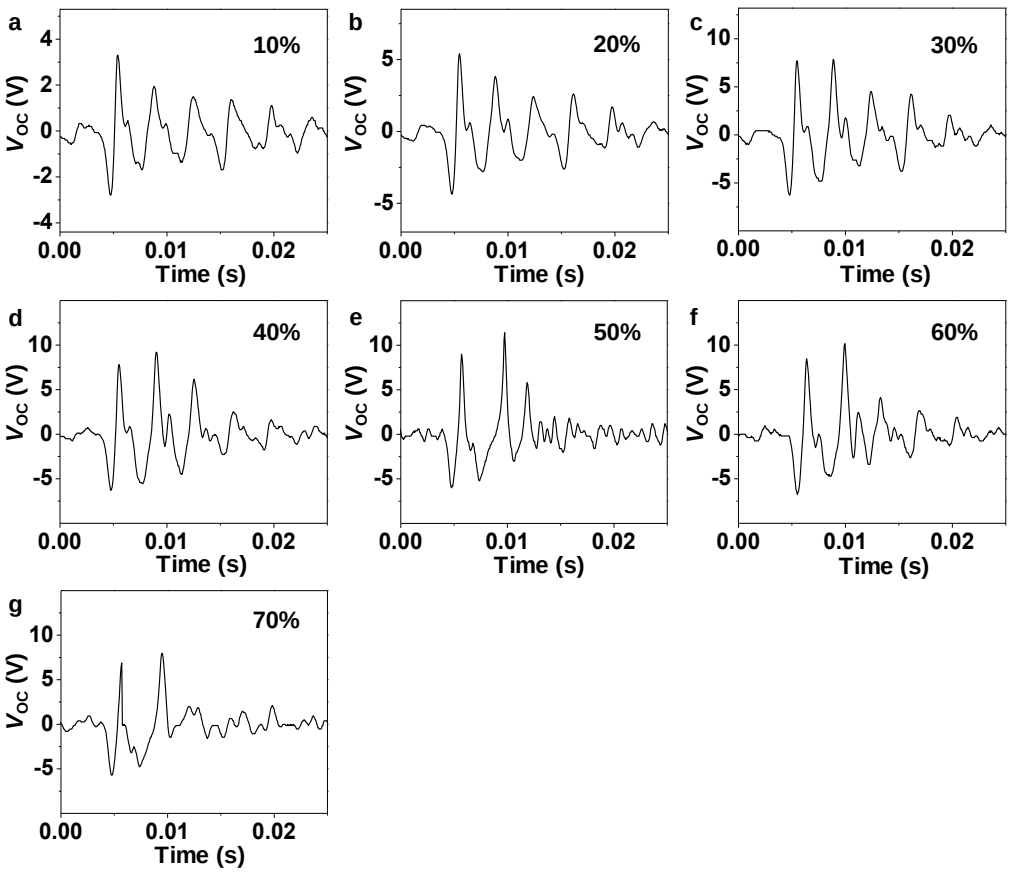

Figure S8. The voltage outputs generated during one impact of the oscillator from nanoporous PVDF thin films fabricated using different ZnO mass fraction mixtures from 10% to 70%, respectively. All the voltage data were collected under the frequency of 40 Hz.

Table S1. Spring constant K and total damping ratio C_{total} values of PVDF thin films with different porosities prepared from the mixtures at varying ZnO mass fraction.

ZnO mass fraction	10%	20%	30%	40%	50%	60%	70%
K (N/V)	32×10^4	30×10^4	25×10^4	9×10^4	7.1×10^4	4.8×10^4	4.4×10^4
C_{total} (N s/V)	715	768	839	939	926	1047	1416

S6. The output voltage of the NG at different oscillation frequencies

The output voltage signals of the PVDF NG were obtained at oscillation frequencies ranging from 20 to 60 Hz, as shown in Figure S9. The PVDF NG produced stable voltage outputs under different oscillation frequencies. The peak voltage was almost independent to the oscillation frequencies. This demonstrated that the NG is able to work at range of common oscillation frequencies found in ambient environment.

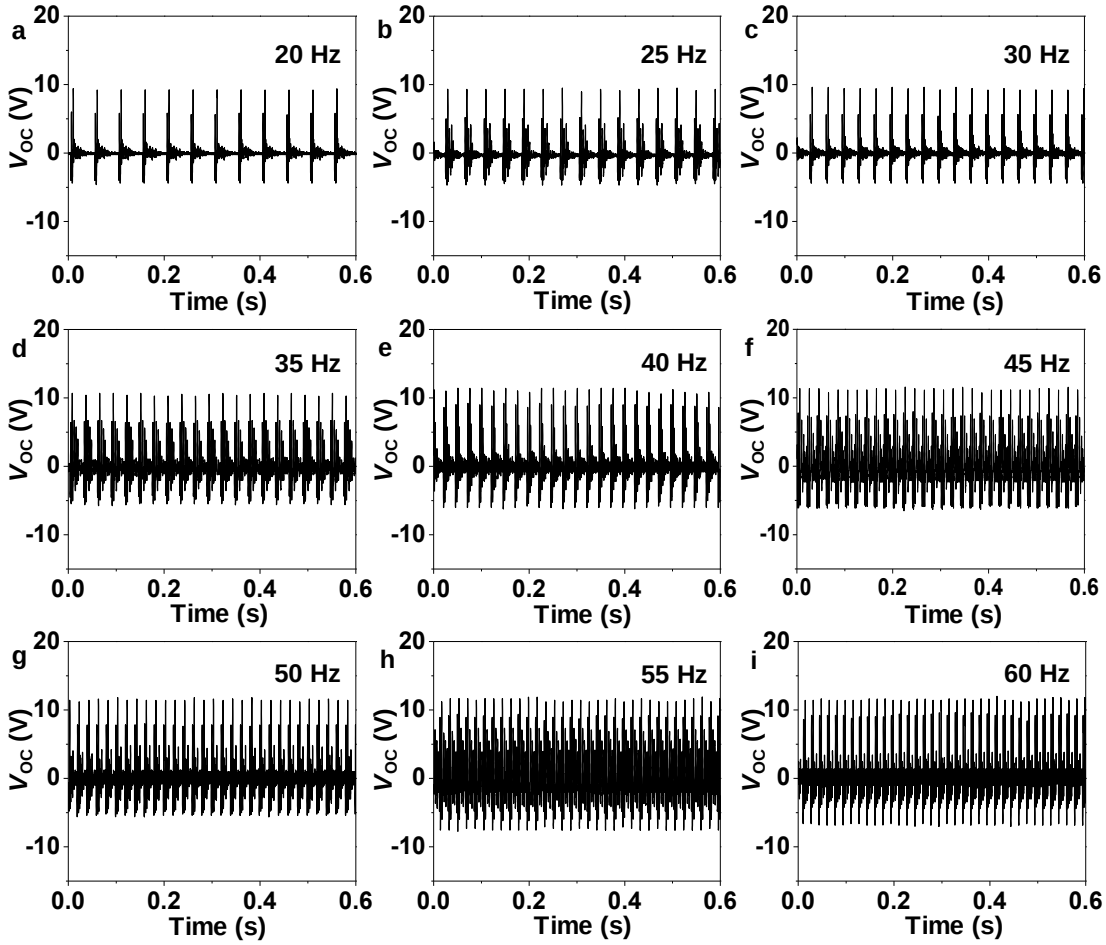

Figure S9. Voltage responses of the nanoporous PVDF thin film to a range of varying frequencies.

S7. Rectified voltage output of the NG

A full-wave bridge circuit composed of four diodes was used to rectificate the AC output into DC signal. Figure S10a shows the voltage output of the NG after rectification under an oscillation frequency of 40 Hz. Figure S10b is the enlarged view of the voltage signal for one oscillation in Figure S10a. The voltage output of the PVDF NG was fully rectified by the bridge circuit with negligible decrease in the peak amplitude.

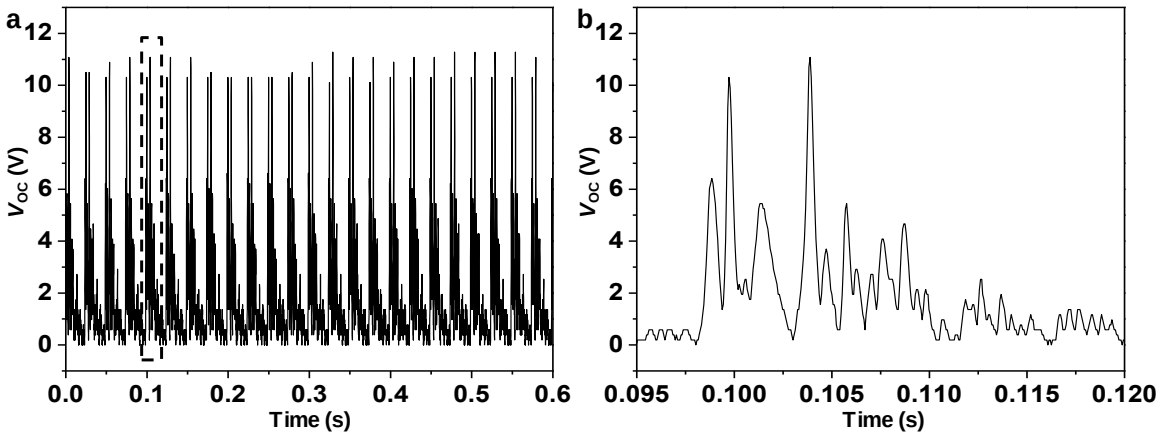

Figure S10. a) The voltage output of the NG after rectification under an oscillation frequency of 40 Hz. b) The enlarged view of the selected area shown in a showing the voltage profile within one oscillation cycle.

S8. Integration of PVDF NGs as a practical power source

Four parallel connected PVDF NGs were taped on the back of a smart phone, and the output signals were measured during the oscillation with a triggering frequency of 40 Hz (see Video S1). The output power were rectified by a bridge circuit and stored in a 47 μF capacitor. The charging feature of the capacitor under an oscillation frequency of 40 Hz was shown in Figure S11, which was charged by the phone-NGs system. The voltage maintained on the capacitor can be reached to 3.7 V in 38 min. Two 47 μF capacitors were charged by connecting in parallel first, and then the capacitors were switched to series connections to increase the output voltage. After combining a predesigned 5 V voltage regulator, the generated electrical energy can activate the turning on of the smart phone by itself (Video S2).

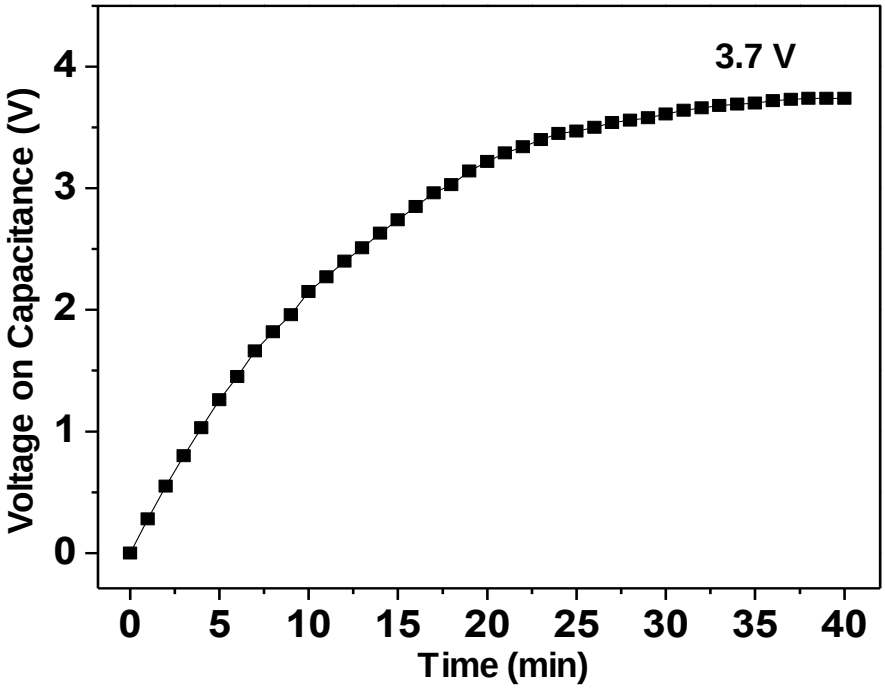

Figure S11. Charging curve of a 47 μF capacitor charged through four parallel connected NGs operated by a smart phone under an oscillation frequency of 40 Hz.

Video S1. Four parallelly connected NGs were integrated onto the back surface of a smart phone and operated by the phone's own weight under an oscillation frequency of 40 Hz.

Video S2. The electrical energy generated by the integratable NGs activated the turning on of the phone.

References

[1] A. Salimi, A. A. Yousefi, *Polym. Test.* **2003**, *22*, 699.

[2] J. F. Zheng, A. H. He, J. X. Li, C. C. Han, *Macromol. Rapid Commun.* **2007**, *28*, 2159.